Description of chiral doublets in $A\sim130$ nuclei and the possible chiral doublets in $A\sim100$ nuclei

J. Peng,[1] J. Meng,[1,2,3,*] and S. Q. Zhang[1]
[1]*School of Physics, Peking University, Beijing 100871, China*
[2]*Institute of Theoretical Physics, Chinese Academy of Science, Beijing 100080, China*
[3]*Center of Theoretical Nuclear Physics, National Laboratory of Heavy Ion Accelerator, Lanzhou 730000, China*
(Received 30 April 2003; published 31 October 2003)

The chiral doublets for nuclei in $A\sim100$ and 130 regions have been studied with the particle-rotor model. The experimental spectra of chiral partner bands for four $N=75$ isotones in $A\sim130$ region have been well reproduced by the calculation with the configuration $\pi h_{11/2}\otimes\nu h_{11/2}^{-1}$. The possible chiral doublets in $A\sim100$ region have been predicted by the particle-rotor model with the configuration $\pi g_{9/2}\otimes\nu g_{9/2}^{-1}$ based on the analysis of the spectra, the $\omega-I$ relation, the $B(M1)$ and $B(E2)$ transition probabilities, and the structure of the wave functions. The possible chiral doublets for nuclei with asymmetric particle and hole configurations are also discussed.

DOI: 10.1103/PhysRevC.68.044324 PACS number(s): 21.10.Re, 21.60.Cs, 21.60.Ev

I. INTRODUCTION

Static chiral symmetries exist commonly in nature. We can find many examples including the macroscopic spirals of snail shells and the microscopic handedness of certain molecules. In particle physics, it is a dynamic property distinguishing between the parallel and antiparallel orientations of the intrinsic spin with respect to the momentum of the particle. In nuclear physics, triaxially deformed doubly odd nuclei can rotate in a left-handed and right-handed geometrical configuration, which is the manifestation of chiral symmetry breaking predicted recently [1]. The angular momenta of the core and of the odd particles can form either a left-handed or a right-handed combination. These two possibilities are transformed into each other by the chiral operator which combines time reversal and rotation by 180°, $\chi=\mathcal{TR}(\pi)$, instead of any other simple rotation. In the ideal case, the two equivalent chiral arrangements are independent with each other, and we can get two degenerate bands with the same quasiparticle configuration.

In Ref. [1], a pair of $\Delta I=1$ bands found in ^{134}Pr($N=75$), with the $\pi h_{11/2}\otimes\nu h_{11/2}^{-1}$ configuration [2], has been suggested as a candidate for the chiral doubling. Recently, the possible experimental evidences are reported for a series of chiral twin bands in odd-Z $N=75$ isotones (^{130}Cs, ^{132}La, ^{134}Pr, ^{136}Pm) [3] and $N=73$ isotones (^{128}Cs, ^{130}La, ^{132}Pr) [4]. Hartley *et al.* [5] reported the chiral doublet bands in ^{136}Pm, and compared the calculated transition strength ratios $B(M1)/B(E2)$ of the chiral bands with the experimental values for the first time. Using a phenomenological core-particle-hole coupling model similar to that in Ref. [1], the chirality in odd-odd nuclei has been studied based on the configuration $\pi h_{11/2}\otimes\nu h_{11/2}^{-1}$ and compared with the experimental data, more details can be found in Refs. [6–8] and the references therein. In the mass region $A\sim130$, there are many other experimental evidences [9–12] which support the existence of the chiral doublet bands in triaxially deformed doubly odd nuclei. Furthermore, the first chiral bands in the even-even nucleus have been observed in ^{136}Nd recently [13].

On the theoretical side, such chiral bands have been predicted by the particle-rotor model (PRM) and tilted axis cranking (TAC) model based on the mean field approximation for triaxial deformed case [1]. The breaking of the chiral symmetry is due to the fact that the axis of the uniform rotation lies outside any of the principal plane of the density distribution. The semiclassical mean field description for tilted nuclear rotation can be traced back to 1980s [14–16]. The qualities of the TAC approximation have been discussed and tested in Ref. [17] with the PRM model. A detailed discussion of the self-consistent tilted axis cranking approach can be found in Ref. [18]. The advantage of the mean field approach is that it can be easily extended to the multiquasiparticle case. However, the mean field approach violates the rotational invariance and the total angular momentum is not a good quantum number. The chiral doublet bands are the results of the TAC in the triaxial case and can be observed experimentally due to the breaking of the chiral symmetry by quantum tunneling effect, as demonstrated in PRM. Although much effort has been devoted to study the TAC phenomena, the more microscopic relativistic mean field model and Skyrme–Hartree-Fock calculations have been reported only in the context [19,20] of planar rotation, i.e., magnetic rotation, due to their sophisticated codes and time consuming numerical procedures. In Ref. [21], using hybrid Woods-Saxon and Nilsson model to replace the single-particle energies in the triaxial TAC model of Ref. [1] and combining with shell correction method, the existence of chiral characteristic for ^{134}Pr and ^{188}Ir has been demonstrated.

In this paper, the chiral doublet structures for nuclei in $A\sim100$ and 130 regions will be studied with the particle-rotor model. The rotational levels $B(M1)$ and $B(E2)$ and the total angular momentum as a function of the rotational frequency will be presented to analyze the properties of the chiral doublet bands. The chiral doublet bands observed in $A\sim130$ region will be described and in $A\sim100$ region will be predicted.

*Email address: mengj@pku.edu.cn

II. FORMULATION

To describe the interplay between the motion of particles and the collective motion, Bohr and Mottelson proposed to take into account only a few so-called valence particles, which move more or less independently in the deformed well of the core, and to couple them to a collective rotor which stands for the rest of the particles [22]. The division into core and valence particles is not always unique. Generally, one divides the Hamiltonian into two parts: an intrinsic part H_{intr}, which describes microscopically a valence particle or a whole subgroup of particles near Fermi level; and a phenomenological part H_{coll}, which describes the inert core.

The total PRM Hamiltonian is written as

$$H = H_{intr} + H_{coll}. \tag{1}$$

Here, we consider the case of a proton particle p and a neutron hole n in the intrinsic channel, i.e.,

$$H_{intr} = h_p + h_n. \tag{2}$$

The formalism can be extended to the multiproton or multineutron cases.

For a single-j model, the quadrupole deformation potential which results in the energy level splitting is

$$V_p = \frac{206}{A^{1/3}}\beta\left[\cos\ \gamma Y_{20} + \frac{\sin\ \gamma}{\sqrt{2}}(Y_{22} + Y_{2-2})\right]. \tag{3}$$

The corresponding single-particle energy for a single-j model can be obtained as

$$h_{p(n)} = \pm\frac{1}{2}C\left\{\left(j_3^2 - \frac{j(j+1)}{3}\right)\cos\ \gamma + \frac{1}{2\sqrt{3}}[j_+^2 + j_-^2]\sin\ \gamma\right\}, \tag{4}$$

where the plus sign refers to a particle, the minus to a hole, and the coupling constant C is

$$C = \frac{195}{j(j+1)}A^{-1/3}\beta\ \text{MeV}. \tag{5}$$

The angular momentum operators of the core ($\vec{R}$) and of the valence particles ($\vec{j}$) form the total angular momentum $\vec{I}$,

$$\vec{I} = \vec{R} + \vec{j}_p + \vec{j}_n. \tag{6}$$

For the case of the triaxial rotation, the moments of inertia for irrotational flow are

$$\mathcal{J}_\nu = \mathcal{J}\sin^2\left(\gamma - \frac{2\pi}{3}\nu\right)(\nu = 1, 2, 3), \tag{7}$$

where $\mathcal{J}$ depends on the quadrupole deformation β and the mass parameter [23]. Usually, the moment of inertia increases with the angular momentum. For simplicity, a constant moment of inertia is assumed in the calculation.

The Hamiltonian of the core is

$$H_{coll} = \sum_{\nu=1}^{3}\frac{(\hat{I}_\nu - \hat{j}_\nu)^2}{2\mathcal{J}_\nu}. \tag{8}$$

The total Hamiltonian (1) is invariant under 180° rotations about the intrinsic axes (D_2 symmetry group). So the eigenvectors of PRM Hamiltonian can be written [24] as

$$|IM\alpha\rangle = \sqrt{\frac{1}{2(1+\delta_{K0})}}\left\{\sum_{K,k_p,k_n} C_{k_pk_n}^{IK\alpha}[|IMKk_pk_n\alpha\rangle + (-1)^{I-j_p-j_n}|IM-K-k_p-k_n\alpha\rangle]\right\}, \tag{9}$$

where $|IMK\rangle$ is the Wigner D function, $|k_pk_n\rangle$ is the product of the proton and neutron states $|jk\rangle$, $C_{k_pk_n}^{IK\alpha}$ is the expansion coefficient, and the summation is restricted to $|K|\leqslant I$, $|k_i|\leqslant j_i$, $(i=n,p)$, $(K-k_p-k_n)$ even, $k_p+k_n>0$, when $k_p+k_n=0$, $k_p\geqslant 0$. The angular momentum projections onto the quantization axis (3-) in the intrinsic frame and the z axis in the laboratory frame are denoted by K and M, respectively, and the other quantum numbers are denoted by α.

The reduced transition probabilities are defined as

$$B(\sigma\lambda, I'\alpha' \to I\alpha) = \sum_{M'M}|\langle \mathrm{f}, IM\alpha|\hat{T}_{\lambda\mu}|\mathrm{i}, I'M'\alpha'\rangle|^2, \tag{10}$$

where $\sigma=E$ or M indicates electric or magnetic transition, respectively, and λ is the rank of electric or magnetic transition operator from initial state i to final state f.

The quadrupole moments in the intrinsic system and the laboratory frame are connected by the relation

$$\hat{Q}_{2\mu} = \mathcal{D}_{\mu0}^{2*}\hat{Q}'_{20} + (\mathcal{D}_{\mu2}^{2*} + \mathcal{D}_{\mu-2}^{2*})\hat{Q}'_{22}, \tag{11}$$

where $\hat{Q}_{2\mu}$ and $\hat{Q}'_{2\mu}$ are the transition, operators of the core in the laboratory frame and the intrinsic frame, respectively. For the stretched $E2$ transitions we have

$$B(E2, I\alpha \to I'\alpha') = Q_0^2\frac{5}{16\pi}\left|\sum_{K,K'}^{k_p,k_n} C_{k_pk_n}^{IK\alpha}C_{k_pk_n}^{I'K'\alpha'}\left[\cos\gamma\langle IK20|I'K'\rangle - \frac{\sin\gamma}{\sqrt{2}}(\langle IK22|I'K'\rangle + \langle IK2-2|I'K'\rangle)\right]\right|^2, \tag{12}$$

in which the contribution from the single particles is neglected as the Q_0 value is much larger than that from the single particles. $Q_0=(3/\sqrt{5\pi})R_0^2Z\beta$ is the intrinsic charge quadrupole momentum, R_0 the nuclear radius, and Z the charge number.

The $B(M1)$ values are the following:

TABLE I. The parameters in the triaxial PRM calculation. Compared with Ref. [3], the same γ value is taken and the parameter C is comparable with ε. ($\varepsilon\approx0.95\beta$).

	$^{130}_{75}$Cs	$^{132}_{75}$La	$^{134}_{75}$Pr	$^{136}_{75}$Pm
C(MeV)	0.175	0.19	0.19	0.21
ε[3]	0.16	0.175	0.175	0.195
γ[3]	−39	−32	−27	−27

$$
\begin{aligned}
&B(M1, I\alpha \to I'\alpha') \\
&= \frac{3}{16\pi}\Bigg| \sum_{\mu,k_p,k_n,k'_p,k'_n} \frac{1}{(1+\delta_{K'0})}\frac{1}{(1+\delta_{K0})} \\
&\times C^{IK\alpha}_{k_p k_n} C^{I'K'\alpha'}_{k'_p k'_n} [\langle IK1\mu | I'K'\rangle \\
&\times \langle k'_p k'_n | (g_p - g_R) j_{p\mu} + (g_n - g_R) j_{n\mu} | k_p k_n\rangle \\
&+ (-1)^{I-j_p-j_n} \langle I - K1\mu | I'K'\rangle \langle k'_p k'_n | (g_p - g_R) j_{p\mu} \\
&+ (g_n - g_R) j_{n\mu} | -k_p - k_n\rangle] + \text{sign}\Bigg|^2 \qquad (13)
\end{aligned}
$$

where sign represents the contribution due to the symmetry of state $|IM\alpha\rangle$ in Eq. (9), which is the same as the first two terms in Eq. (13) by the replacement $K' \to -K'$, $k'_p \to -k'_p$, and $k'_n \to -k'_n$. The spherical tensor of rank-1 j_μ is

$$
j_\mu = \left(j_0 = j_3, j_{\pm1} = \frac{\mp(j_1 \pm i j_2)}{\sqrt{2}} \right). \qquad (14)
$$

III. RESULTS AND DISCUSSIONS

For the numerical calculation, we follow the procedures in Ref. [1] to study the chiral doublet structures in $A\sim100$ and 130 nuclei using the particle-rotor model. First, the rotational spectra of these four isotones in $A\sim130$ nuclei in Ref. [3] are calculated and compared with the experimental data. We fix the configuration as $\pi h_{11/2}\otimes\nu h^{-1}_{11/2}$ and $\mathcal{J}$ =25 MeV^{-1}. The parameters in our calculation are listed in Table I. Second, the proton and neutron configuration $\pi g_{9/2}\otimes\nu g^{-1}_{9/2}$ is adopted in the calculation of $A\sim100$ nuclei with $\mathcal{J}$=30 MeV^{-1}, γ=−30°, and C=0.1 MeV, 0.20 MeV, 0.25 MeV corresponding to the deformation $\beta\approx0.06$, 0.12, 0.15, respectively. In the calculation of $B(M1)$ and $B(E2)$, the quadrupole moments Q'_{21} and Q'_{2-1} are zero in the intrinsic frame by definition. Since we are only interested in the trends of the $B(M1)$ and $B(E2)$ instead of the absolute values of $B(M1)$ and $B(E2)$, the g factors $g_{p(n)}-g_R$ are set as 1 or −1 for the proton or neutron, respectively, and the intrinsic quadrupole moments are chosen as $Q'_{20}=\cos\gamma$, $Q'_{22}=Q'_{2-2}=-\sin\gamma/\sqrt{2}$. Finally, the chiral doublet structures with asymmetric particle-hole configuration $\pi g^{-1}_{9/2}\otimes\nu h_{11/2}$ in ^{104}Rh are also discussed.

For γ=−30°, we have the axial length relation $R_1<R_2<R_3$ and denote the intrinsic axes 1, 2, and 3 as the s, i, and l axes, respectively [22]. The moment of inertia as a function of γ-deformation is presented in Fig. 1. When γ=−30°, one has $\mathcal{J}_l=\mathcal{J}_s=\frac{1}{4}\mathcal{J}_i$, i.e., the collective angular momentum vector $\vec{R}$ tends to align along the intermediate axis, which minimizes the rotational energy [22]. The single-particle and -hole angular momentum vectors will tend to align along the short and long nuclear axes, respectively. These three angular momenta are mutually perpendicular to each other. These orientations maximize the overlap of the particle densities with the triaxial potential, and result in minimizing the interaction energy [1].

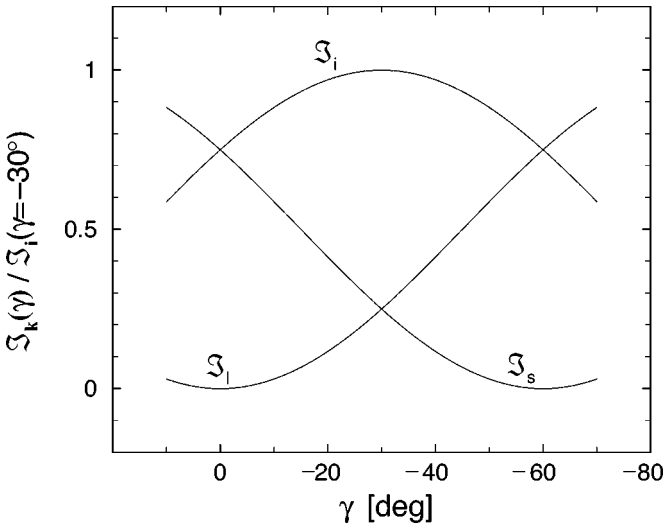

FIG. 1. The moments of inertia for irrotational flow as functions of γ deformation.

The four pairs of chiral doublet bands have been observed in $A\sim130$ region [3]. The observed and the calculated energy spectra for ^{130}Cs, ^{132}La, ^{134}Pr, and ^{136}Pm are presented in Fig. 2. The configuration $\pi h_{11/2}\otimes\nu h^{-1}_{11/2}$ and the moment of

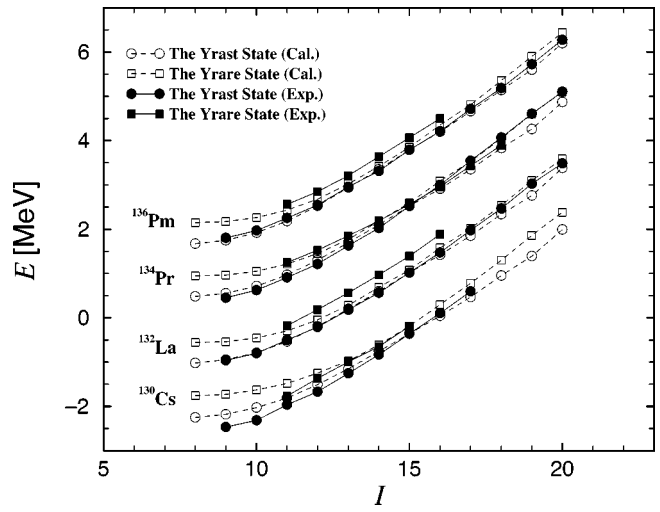

FIG. 2. Calculated and experimental energies for yrast band (circles) and yrare band (squares) with the configuration of $\pi h_{11/2}\otimes\nu h^{-1}_{11/2}$ in four N=75 isotones ^{130}Cs, ^{132}La, ^{134}Pr, and ^{136}Pm. The open symbols correspond to the calculated values. The filled symbols correspond to the experimental values. For the details, see the text.

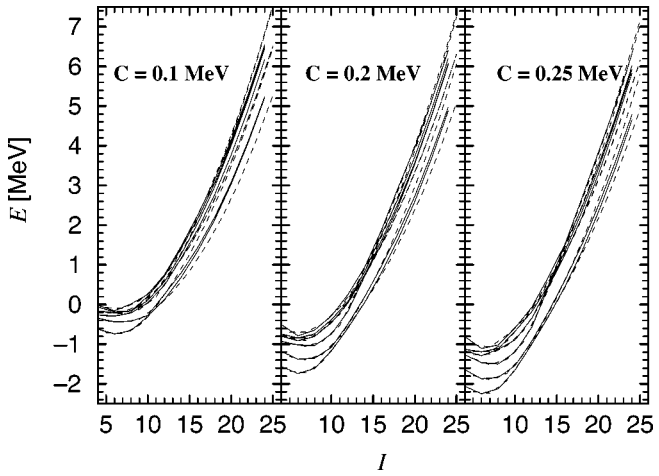

FIG. 3. Rotational energies vs total angular momentum for the configuration $\pi g_{9/2} \otimes \nu g_{9/2}^{-1}$ calculated with $\mathcal{J}=30$ MeV^{-1}, $\gamma=-30°$, and different C values. Full lines correspond to even and dashed to odd spin.

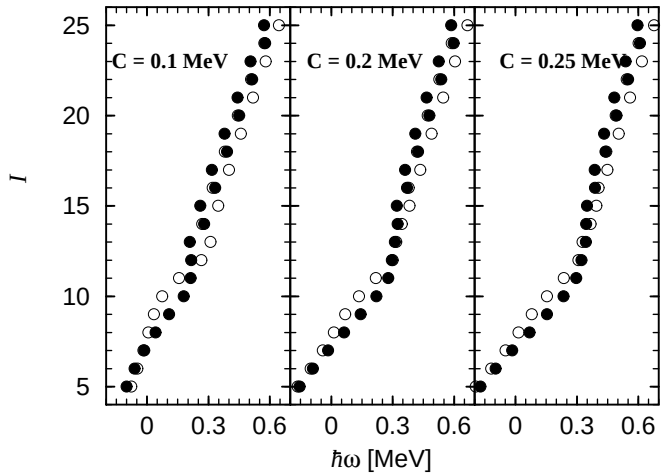

FIG. 4. The total angular momentum as a function of the rotational frequency for the configuration $\pi g_{9/2} \otimes \nu g_{9/2}^{-1}$ calculated with $\gamma=-30°$ and $\mathcal{J}=30$ MeV^{-1}. The filled and open circles represent the yrast and the yrare band, respectively.

inertia of the rotor, $\mathcal{J}=25$ MeV^{-1}, have been chosen in the calculation. The available data and also the recommended bandhead spin ($I=9\hbar$) are taken from Ref. [3]. According to the ε deformation of three-dimensional TAC calculation [3], the corresponding parameters C are chosen as in Table I. Similar as in Ref. [3], the calculated spectra are separated by 1.5 MeV for display. The data of ^{130}Cs, ^{132}La, ^{134}Pr, and ^{136}Pm are shifted by −2.47 MeV, −0.96 MeV, +0.45 MeV, and +1.80 MeV, respectively. In such a way, the calculated energies are set to be equal to the experimental data at $I=15\hbar$, so that the experimental and the calculated spectra can be compared easily. In Fig. 2, the calculated and observed energy levels are coincident with each other and both show the energy degeneracy around $I=15\hbar$ for ^{134}Pr. For the other $N=75$ isotones, the sidebands are displaced modestly in energy from the yrast bands. For ^{130}Cs, this displacement stays roughly constant at $\approx$0.22 MeV in the data and at $\approx$0.25 MeV in the calculated data, respectively, in the spin interval $11\hbar<I<15\hbar$. There is a relatively large energy displacement between chiral bands in ^{132}La and ^{136}Pm. It is shown that the chiral doublet bands observed in $A\sim130$ nuclei can be well understood from the PRM, similar to that in Refs. [6,7]. The mutual orientation of angular momentum components has also been studied and the same conclusion as Refs. [6,7] has been drawn, namely, the spontaneous chiral symmetry breaking leads to the doubling of states.

After the discussion for $A\sim130$ nuclei, we wonder whether the chiral doublets exist in $A\sim100$ nuclei with the configuration $\pi g_{9/2} \otimes \nu g_{9/2}^{-1}$.

For the $A\sim100$ nuclei, the rotational bands obtained from the PRM Hamiltonian with $\mathcal{J}=30$ MeV^{-1} and $\gamma=-30°$ are presented in Fig. 3. The left, middle, and right panels correspond to the case of $C=0.1$ MeV, 0.2 MeV, and 0.25 MeV, respectively. The combination of the proton particle with the neutron hole favors the s-l plane. At the beginning of the bands, the collective angular momentum $\vec{R}$ is small and the total angular momentum $\vec{I}$ lies in a principal plane defined by the short and long principal axes of the deformed nucleus. There are two degenerate solutions (planar solution) obtained by the rotation $R_3(\pi)$[or $R_1(\pi)$] that can be combined into degenerate states of opposite signature, similar to that in Ref. [1]. In all the panels of Fig. 3, the characteristic of $\Delta I=1$ bands appears in low lying states before $I=11\hbar$. With the spin increasing, $\vec{R}$ becomes comparable to the single-particle angular momentum, $\vec{I}$ gradually turns towards the i axis and does not lie in any of the principal plane. This is demonstrated in all of the three panels of Fig. 3 with the two lowest bands becoming nearly degenerate around $I=12\hbar$. In the left panel, the yrast band and the yrare band are close to each other near $I=12\hbar$ despite the fact that the overall energy displacement between the two lowest bands is relatively large. In the middle panel, the two lowest bands become nearly degenerate near the spin interval $11\hbar<I<13\hbar$. The interval of energy degeneracy is $11\hbar<I<15\hbar$ in the right panel. This shows that the chiral symmetry favors the case with larger deformation. After $I=15\hbar$, the degenerate energy band splits into four bands with $\Delta I=2$. The near degeneracy for the pairs of $\Delta I=1$ bands give the signal that chiral doublet bands exist in $A\sim100$ nuclei with the configuration $\pi g_{9/2} \otimes \nu g_{9/2}^{-1}$.

From the PRM energies in Fig. 3, the frequency can be calculated by means of $\omega(I)=[E(I+1)-E(I-1)]/2$ [17]. The functions $I(\omega)$ are presented in Fig. 4. The deformation parameter C in the left, middle, and right panels is taken as 0.1 MeV, 0.2 MeV, and 0.25 MeV, respectively, as in Fig. 3. In Fig. 4, when $I<8\hbar$, the frequency ω is negative because the total angular momentum near the bandhead is mainly provided by the orientation of the particle and the hole. This is the region where the classical mean field approximation does not work. The negative rotational frequency means that the rotation is not the collective rotation usually assumed in cranking approximation but intrinsic excitations. When $8\hbar \leqslant I \leqslant 12\hbar$ ($0 \leqslant \hbar\omega \leqslant 0.3$ MeV), the total angular momentum is provided by the single particle and the hole together with the core. The rotation is aplanar. The bands in this spin region show up as a nearly straight line in all three panels of Fig. 4.

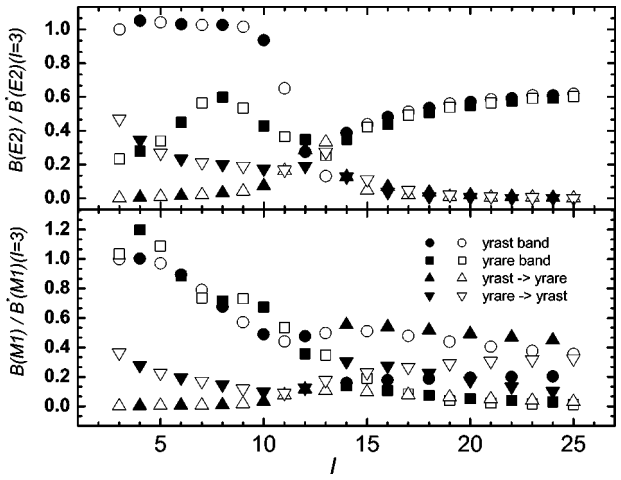

FIG. 5. $B(M1)$ and $B(E2)$ values as functions of the total angular momentum for a $g_{9/2}$ particle and a $g_{9/2}$ hole coupled to a triaxial rotor with $\gamma=-30°$. $B^*(M1)(I=3)$ and $B^*(E2)(I=3)$ are, respectively, the intraband $B(M1)$ and $B(E2)$ transitions of the yrast band at $I=3\hbar$. The filled symbols correspond to the even spin, while the open ones to the odd spin. The symbols, circles, squares, triangle ups and triangle downs represent, respectively, the intraband transitions of the yrast band, the intraband transitions of the yrare band, the interband transitions from the yrast band to the yrare band, and the interband transitions from the yrare band to the yrast band.

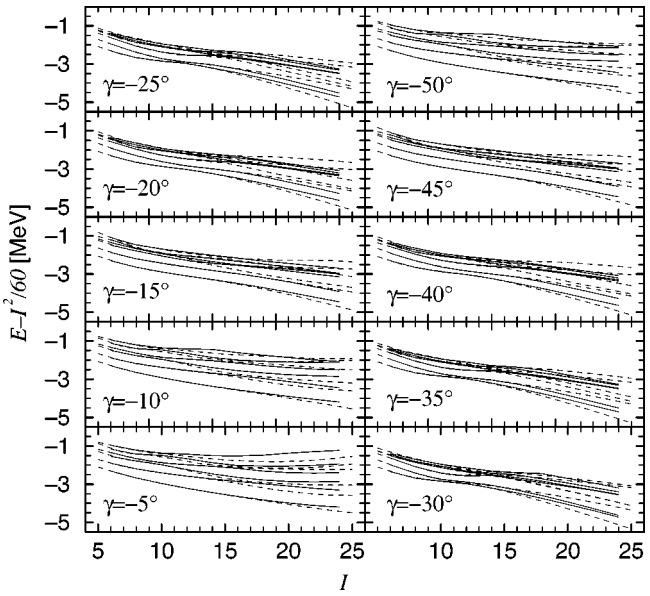

FIG. 6. Rotational bands of a $g_{9/2}$ proton particle and a $g_{9/2}$ neutron hole coupled to a triaxial rotor with $C=0.2$ MeV and $\mathcal{J}=30$ MeV^{-1}. Different values of $\gamma(-5°,-10°,\ldots,-50°)$ are taken in the calculation. Full lines correspond to even and dashed to odd spin.

For higher spins, the core becomes dominant to contribute to the total angular momentum and the angular momentum will align along the i axis, leading to the kink of the second kind of the moment of inertia $\mathcal{J}^{(2)}=dI(\omega)/d\omega$ (see Fig. 4), which is the slope of the curve $I(\omega)$. This kink represents a reorientation of the total angular momentum from the aplanar towards the i axis. After the kink, the angular momenta of the core and the single particles will align along the intermediate axis, which is the direction of the total angular momentum, and the signature splitting appears. It should be noted that the stability of chiral geometry depends on the competition between strength of the single-particle Hamiltonian and the Coriolis force whose strength is related to the moment of inertia. The signature splitting should not appear if chiral geometry is always stable.

In order to study chiral doublet structures, the reduced $B(M1)$ and $B(E2)$ transition probabilities are presented in Fig. 5 for the case of $C=0.2$ MeV and $\mathcal{J}=30$ MeV^{-1}. Since we are only interested in the trends of the $B(M1)$ and $B(E2)$, the transition values in Fig. 5 are given in the units of the $B(M1)$ and $B(E2)$ yrast intraband transitions at $I=3\hbar$, respectively. The upper panel shows the $B(E2)$ transition probabilities, and the lower panel corresponds to the $B(M1)$ values. The filled symbols and the open symbols represent the transition probabilities of the bands with even spin and odd spin, respectively. The interband transition probabilities reflect the change from the planar to the aplanar rotation [1]. At low spins, it is the case of planar rotation, and there are weak interband transitions but strong intraband transitions in Fig. 5. Near $I=12\hbar$, where the two bands come very close and the rotation becomes aplanar, the interband transitions in both directions are observed. At the crossing point, the two intrinsic structures are mixed, and the interband $B(E2)$ transition is larger than the intraband $B(E2)$ transition. After $I=15\hbar$, the rotation rapidly aligns towards the principal i axis. There appears the spin-dependent splitting in the level energies. The $B(E2)$ transition is not affected by this splitting. This is a regular electric transition between $\Delta I=2$ bands as shown in the upper panel of the Fig. 5. Moreover, it is observed that the inter band $B(E2)$ transitions disappear. After $I=15\hbar$, the calculated $B(M1)$ transition in the lower panel of the Fig. 5 shows odd-even staggering. The dominant $B(M1)$ transition appears for the intraband of the yrast band with odd spin and for the interband (yrast band to yrare band) with even spin. The above conclusions are consistent with $B(M1)/B(E2)$ staggering discussed for the partner bands in Refs. [8,25].

To find out the range of γ deformation for the appearance of chiral doublet bands, the calculated level energies for a particle and a hole coupled to the triaxial rotor with different γ values are shown in Fig. 6, similar to that in Refs. [1,6] but for different configuration. We find that the chiral doublet bands appear in the interval $-35°<\gamma<-25°$. It should be noted that the difference between yrast bands and yrare bands has been amplified by subtracting a rotor energy $I^2/60$ MeV. In most cases, the energy difference is within 0.7 MeV. It indicates that there is a certain margin of the γ −deformation, where the energy degeneracy is expected. The best condition for the appearance of the chiral doublet bands is $\gamma=-30°$ in $A\sim100$ region with the configuration of $\pi g_{9/2}\otimes\nu g_{9/2}^{-1}$, similar to that in Refs. [1,6].

To further investigate the microscopic reasons of chiral doublet bands, the structure of the wave functions for the yrast bands and the yrare bands for the configuration $\pi g_{9/2}\otimes\nu g_{9/2}^{-1}$ are presented in Fig. 7. They are taken from the triaxial PRM calculation with $C=0.25$ MeV, $\mathcal{J}=30$ MeV^{-1}, and $\gamma=-30°$. Here, only the first term in Eq. (9) is adopted to

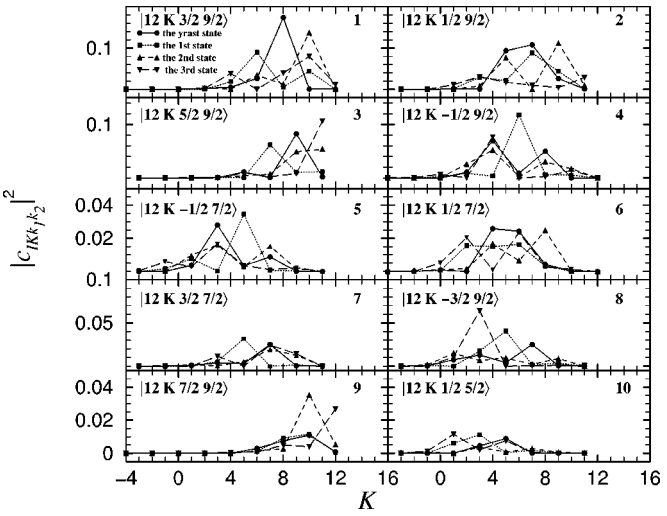

FIG. 7. The main structure of the triaxial PRM eigenstates as a function of the total projection K for C=0.25 MeV, γ=−30°, and I=12$\hbar$. The probabilities of the yrast band, the yrare band, the second excited band and the third excited band, are given by filled circles, filled squares, filled triangles up, and filled triangles down symbols, respectively. The quantum numbers for corresponding basis states are indicated in the upper left corner of each panel.

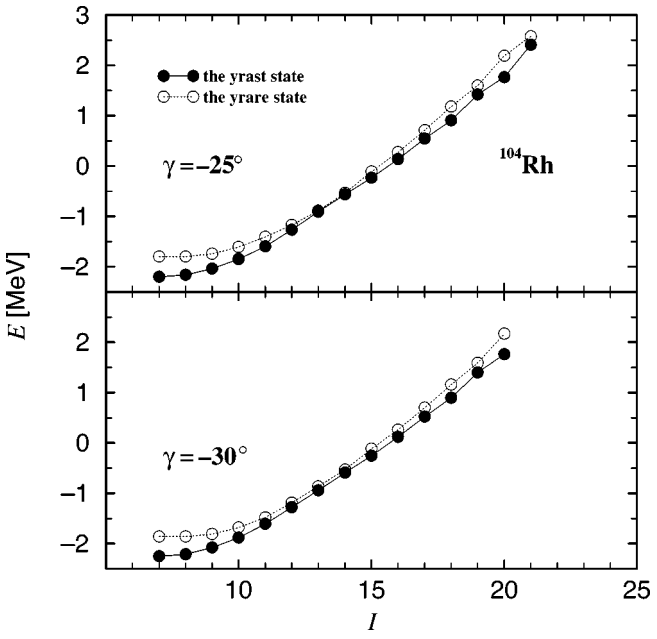

FIG. 8. Rotational spectra for the yrast and yrare bands with the configurations $\pi g_{9/2}^{-1}\otimes\nu h_{11/2}$, C=0.2 MeV, and $\mathcal{J}$=30 MeV^{-1}. The upper and lower panels shows the cases of γ=−25° and γ=−30°, respectively. The filled circles indicate the yrast band, and the open circles indicate the yrare band.

calculate the probability distribution as the function of K. We choose the top ten basis states $|12MKk_1k_2\rangle$ with the largest contribution to the yrast band states. The probability distributions are far more complicated than we have expected. This complexity indicates that the composition of the total angular momentum is not as simple as in the picture of the classical mean field approximation and the quantum effects are very important. Moreover, this complexity may be significantly reduced with different choice of basis states [6]. In Fig. 7, the yrare bands (filled squares) have the similar probability distributions with the yrast bands (filled circles) in many panels. It partly provides the reason why there is energy degeneracy between these two bands. Meanwhile, the quantum effect is so important that the chiral symmetry is broken, as can be seen also in the $B(M1)$ and $B(E2)$ values in Fig. 5.

Recently, Koike *et al.* [25] reported the chiral doublets in ^{104}Rh with the asymmetrical configuration $\pi g_{9/2}^{-1}\otimes\nu h_{11/2}$, which motivated the study of the chiral symmetry breaking in ^{104}Rh here. The energy spectra for yrast and yrare bands with the configurations $\pi g_{9/2}^{-1}\otimes\nu h_{11/2}$, $\mathcal{J}$=30 MeV^{-1}, and C =0.2 MeV are presented in Fig. 8. The corresponding nuclei with such configuration can be found easily in $A\sim100$ region, e.g., ^{104}Rh. The upper and lower panels of Fig. 8 show the calculated energies as a function of spin for γ=−25° and γ=−30°, respectively. In both panels, the two lowest bands are near degenerate in the spin interval $11\hbar<I<16\hbar$. It shows that the chiral doublets exist also in nuclei with asymmetric particle-hole configurations.

IV. CONCLUSIONS

The chiral doublets for nuclei in $A\sim100$ and 130 regions have been studied with the particle-rotor model. The experimental spectra of chiral partner bands for N=75 isotones ^{130}Cs, ^{132}La, ^{134}Pr, ^{136}Pm in $A\sim130$ region [3] have been well reproduced by the calculation with the configuration $\pi h_{11/2}\otimes\nu h_{11/2}^{-1}$. The possible chiral doublets in $A\sim100$ region corresponding to a γ deformation in the interval $-35°<\gamma<-25°$ have been predicted by the PRM model with the configuration $\pi g_{9/2}\otimes\nu g_{9/2}^{-1}$ based on the analysis of the spectra, the ω-I relation, the $B(M1)$ and $B(E2)$ transition probabilities, and the structure of the wave functions. The possible chiral doublets for nuclei with asymmetric particle and hole configurations are also discussed.

ACKNOWLEDGMENTS

This work was partly supported by the Major State Basic Research Development Program under Contract No. G2000077407 and the National Natural Science Foundation of China under Grant Nos. 10025522, 10047001, and 19935030.

[1] S. Frauendorf and J. Meng, Nucl. Phys. **A617**, 131 (1997).
[2] C. M. Petrache, D. Bazzacco, S. Lunardi, C. Rossi Alvarez, G. de Angelis, M. De Poli, D. Bucurescu, C. A. Ur, P. B. Semmes, and R. Wyss, Nucl. Phys. **A597**, 106 (1996).
[3] K. Starosta *et al.*, Phys. Rev. Lett. **86**, 971 (2001).
[4] T. Koike, K. Starosta, C. J. Chiara, D. B. Fossan, and D. R. LaFosse, Phys. Rev. C **63**, 061304(R) (2001).
[5] D. J. Hartley *et al.*, Phys. Rev. C **64**, 031304(R) (2001).
[6] K. Starosta *et al.*, Phys. Rev. C **65**, 044328 (2002).
[7] K. Starosta *et al.*, Nucl. Phys. **A682**, 375c (2001).
[8] T. Koike *et al.*, Phys. Rev. C **67**, 044319 (2003).
[9] R. A. Bark *et al.*, Nucl. Phys. **A691**, 577 (2001).
[10] A. A. Hecht *et al.*, Phys. Rev. C **63**, 051302(R) (2001).
[11] C. M. Petrache *et al.*, Phys. Rev. C **65**, 054324 (2002).
[12] X. F. Li *et al.*, Chin. Phys. Lett. **19**, 1779 (2002).
[13] E. Mergel *et al.*, Eur. Phys. J. A **15**, 417 (2002).
[14] A. K. Kerman and N. Onishi, Nucl. Phys. **A361**, 179 (1981).
[15] H. Frisk and R. Bengtsson, Phys. Lett. B **196**, 14 (1987).
[16] S. Frauendorf, Nucl. Phys. **A557**, 259c (1993).
[17] S. Frauendorf and J. Meng, Z. Phys. A **365**, 263 (1996).
[18] S. Frauendorf, Nucl. Phys. **A677**, 115 (2000).
[19] H. Madokoro, J. Meng, M. Matsuzaki, and S. Yamaji, Phys. Rev. C **62**, 061301 (2000).
[20] P. Olbratowski *et al.*, Acta Phys. Pol. B **33**, 389 (2002).
[21] V. Dimitrov, S. Frauendorf, and F. Dönau, Phys. Rev. Lett. **84**, 5732 (2000).
[22] A. Bohr and B. R. Mottelson, *Nuclear Structure* (Benjamin, New York, 1975), Vol. 2.
[23] J. Meyer-Ter-Vehn, Nucl. Phys. **A249**, 111 (1975).
[24] J. P. Davidson, *Collective Models of the Nucleus* (Academic, New York, 1968).
[25] T. Koike *et al.*, in *Frontiers of Nuclear Structure*, edited by-Paul Fallon and Rod Clark, AIP Conf. Proc. No. 656, (AIP, Melville, N.Y., 2003), p. 160.